A cost-effective, modular, research-grade optical microscope

Authors: Anupam Bharadwaj[1], Ranjan Kalita[2], Amalesh Kumar[1], Anupam Sarma[3], Bithiah G Jaganathan[4], Sunil Kumar[5], Frederik Gorlitz[5], Jonathan Lightley[5], Chris Dunsby[5], Mark Neil[5], Callum Hollick[6], Jeremy Graham[6], P M W French[5], and Bosanta R Boruah[1].

1. *Department of Physics, Indian Institute of Technology Guwahati, Guwahati 781039, Assam, India*
2. *Department of Physics, Pragjyotish College, Guwahati 781009, Assam, India*
3. *Department of Onco-pathology, Dr. B. Borooah Cancer Institute, Guwahati 781016, Assam, India*
4. *Department of Biosciences and Bioengineering, Indian Institute of Technology Guwahati, Guwahati 781039, Assam, India*
5. *Photonics Group, Department of Physics, Imperial College London, London SW7 2AZ, UK*
6. *Cairn Research Ltd, Graveney Road, Faversham, Kent ME13 8UP, UK*

[1] Email: brboruah@iitg.ac.in

Abstract: *Optical microscopy is a ubiquitous tool in the physical and life sciences and in histopathology where visible light microscopy is used to analyse clinical tissue sections on the micron-scale to help diagnose disease. In recent years, there has been a dramatic evolution of microscope technologies, but these have generally come with increased cost and complexity. To widen access to advanced microscopy capabilities, we are developing a cost-effective modular platform for optical microscopy, (www.openscopes.com). Many of these instruments can be based around a new low-cost and flexible microscope stand, "openFrame", for which the core components are open source. openFrame can support implementations of a wide range of microscope modalities for diverse applications including research, pathology and training. Unlike many commercial microscopes that are often designed for specific applications and cannot easily be upgraded or adapted for different imaging modalities, openFrame-based instruments can be relatively easily maintained, upgraded or adapted to another modality without requiring support from manufacturers. To this end, openFrame-based instruments are envisaged to operate with open-source software, enabling researchers to assemble and modify their own microscopes with minimal challenges presented by proprietary (closed) hardware or software. In this paper, we describe the implementation of a low-cost, research-grade modular optical microscope, applicable to research and pathology.*

Keywords: *Modular optical microscope, affordable, open-source, fluorescence microscopy, pathology*

1. Introduction

Optical microscopes are ubiquitous in the physical and biological sciences, typically using visible electromagnetic radiation for diverse imaging applications in the fields of cell biology [1,2], biotechnology [3,4], life-sciences [5,6], nanotechnology [7,8] and also in the examination of histopathology tissue sections for clinical diagnosis [9–11]. In recent decades, advances in technology have dramatically expanded the capabilities of optical microscopy, driven in part by progress in computational techniques, as well as in light sources and detectors. There is wide interest in implementing advanced microscopy techniques, as well as in exploiting standard instruments for biology and medicine. Most workhorse optical microscopes provide a trans-illumination mode for brightfield imaging. Many offer widefield epifluorescence imaging using LED, lamp or laser sources for fluorescence excitation, and scientific cameras (with sufficient sensitivity for single photon detection) are used for detection A commercial research-grade microscope integrating these modalities typically costs in excess of 5,000,000 Indian Rupees (INR), which can limit access for

scientists in many situations. The capabilities of such a microscope can, however, be realized at significantly reduced cost by assembling a modular instrument from off-the shelf optical, mechanical and electronic components and using open source software. For example, high power solid-state lasers can be replaced with industrial grade diode lasers, and scientific cameras such as EMCCD or sCMOS cameras can be replaced with CMOS machine vision cameras - and newly available lower cost cooled CMOS cameras [e.g., *www.cellcam.co.uk/cameras/*]. Objective lenses with high numerical apertures (e.g., 100X oil immersion, 1.30 N.A.) lenses are available at reasonable cost (< 60,000 INR) and personal computers specified for gaming applications are sufficient for most microscopy image processing. However, the main microscope stand can still be expensive, and proprietary hardware and software may present challenges when implementing a new microscopy technique on a commercial microscope frame. In principle, it is possible to assemble an entire microscope from self-fabricated components, or from generic optomechanical components but this requires significant specific expertise that is beyond most microscope users.

Here we present the implementation in our laboratory at Indian Institute of Technology Guwahati of an optical microscope based on the modular "*openFrame*" microscope stand [12] that is designed to enable non-experts to rapidly configure and assemble research-grade microscopes for a lower component cost than would be required to assemble a microscope entirely from generic commercial optomechanical components. We here report the first translation of the *openFrame* concept from its originating laboratory at Imperial College London [12,13] – to a research laboratory in India – demonstrating broad potential applicability of a modular, self-assembled open microscope to research and clinical pathology. The latest versions of the CAD files for the modules of the basic *openFrame*-based microscope stand are freely shared [12,14] to enable mechanical workshops to fabricate their own components or to get them manufactured locally, or they can be purchased [15].

The basic *openFrame* stand comprises modular anodized aluminum layers that can house optical components such as mirrors, lenses or dichroic beam splitters along a central optical axis, which can be coupled to optomechanical components and devices such as cameras or lasers. The layers are modules that can be assembled to provide a wide range of configurations, including multiple camera ports or fluorescence excitation ports for LED or laser illumination. *openFrame*-based microscopes can be implemented with a manual translation stage to hold and adjust focus of a sample, or it can be configured with motorised module, e.g., utilizing a piezo-electric actuator for axial scanning of the objective lens and a computer controlled motorized x-y stage, e.g., to enable multiwell plate imaging or slide scanning. A trans-illumination pillar can be fitted for brightfield illumination using an LED light source. To date, *openFrame*-based instruments have been applied to fluorescence and quantitative phase imaging [16] and to super-resolved microscopy using

the cost effective *easySTORM* [17] implementation of direct stochastic optical super-resolution microscopy (dSTORM) [1819] that exploits multimode diode lasers delivered by multimode optical fibres for excitation. It has also been adapted to carry out automated microscopy for high content analysis through the use of an open source optical autofocus module[13,20]. The modular *openFrame* concept is relatively compact, enabling it to be installed in confined spaces such as incubators or biosafety confinement facilities, and this makes it convenient to transport the instrument. The implementation of an *openFrame*-based microscope at IIT Guwahati presented in this paper utilizes affordable, industry-grade components. Here we demonstrate its performance both in the trans-illumination and epi–fluorescence modes by imaging a test target, quantum dots and clinical histological specimens.

2. Description of the constituent components and modules of the *openFrame*-based microscope

Most optical microscopes are configured around core components including an objective lens, illumination source, sample stage, eyepiece or camera and microscope stand. To realise this, the *openFrame*-based fluorescence microscope represented in Figure 1 comprises four modular *openFrame* layers plus a base plate, a sample stage adapter and a trans-illumination pillar supporting an LED transillumination source. These layers are rigidly clamped together but their relative orientation can be adjusted in steps of 45 degrees about the optical axis for experimental convenience. Layer 1 is the detection module containing a mirror with its reflecting surface orientated at 45^0 to the vertical optical axis to direct image-bearing light to a camera that can be mounted on the side of the layers. Layer 2 is a "tube lens" module and layer 3 contains the filter cube that introduces the excitation radiation into this fluorescence microscope. Layer 4 supports a mounting for the microscope objective centered on the *openFrame* optical axis. This mounting includes a piezo-electric actuator (Physik Instrumente, Q.545, used with E-873 controller) that translates the microscope objective axially, i.e., along the vertical Z direction. A sample stage adapter layer is mounted on top of the (objective lens) layer 4, onto which a motorized X-Y microscope stage is mounted. A transillumination pillar is also fixed at one of the edges of the stage adapter layer. This system is computer controlled using the open-source *μManager* programme [21] and enables imaging in the trans-illumination or epi-fluorescence modes. Below we provide details of the specific components used in this *openFrame*-based microscope along with a rendering of the CAD representation of the *openFrame* modular stand.

(A) **Trans-illumination for brightfield imaging**: The trans-illumination pillar as seen in Figure 1 is an inverted L shaped stand with an LED source (MONOLED, Cairn Research Ltd), along with a condenser lens of NA=0.34,

attached to its horizontal arm. The pillar is fixed to the X-Y stage adapter. The horizontal arm of the pillar can be translated vertically to adjust the illumination at the sample plane. The light transmitted through the sample in trans-illumination mode is detected by a camera mounted to layer 1 after passing through layers $4 \rightarrow 2$ and being reflected at the 45^0 mirror in layer 1.

(B) **X-Y microscope sample stage**: A motorized X-Y stage (ASR100B120B-E03T3A, Zaber) is installed on a stage adapter layer that is bolted onto layer 4. The X-Y stage can be controlled via a PC running the hardware-software integration (X-MCB2-KX14BG controller, Zaber Console software). It is also possible to control the stage with a joystick (X-JOY3-PTB2, Zaber).

(C) **Objective lens focusing**: Layer 4 contains the objective lens which is mounted on an L-bracket to be centered on the vertical *openFrame* optical axis. To adjust the focusing of the microscope, the objective lens bracket is fitted to a linear precision piezo-electric stage with an encoder providing 1 nm resolution (Q-545.140, Physik Instrumente). The stage controller (E-873 PI Shift Controller, Physik Instrumente) is programmed using the software, PI MikroMove, controlled by *μManager*. In our work, we have used three microscope objective lenses: PLN 20X 0.40 N.A., (Olympus Optical), PlanF 40X 0.75 N.A., (AmScope) and PlanF 100 X oil immersion 1.3 N.A., (AmScope). This *openFrame* layer can also accommodate a dichroic beam splitter that can be used to introduce an infrared laser beam for an optional autofocus module or to implement other functionality [13].

(D) **Fluorescence excitation**: Layer 3 houses the excitation filter cube and has side ports onto which the optical systems for coupling in the excitation light can be mounted. In this implementation, layer 3 has a mechanical slider that can accommodate two filter cubes containing dichroic beam splitters that reflect the radiation entering from the side port up through the objective lens to the sample and transmit the fluorescence emission down towards layer 1 and the camera. Each filter cube contains excitation, dichroic and emission filters. Typically, we use a multiline dichroic filter that enables multiple fluorescence excitation wavelengths to be used. If one cube position is left empty, then the mechanical slider can be set to allow the transmitted light to pass through layer 1 to camera for brightfield imaging. Alternatively, in place of a mechanical slider, a single filter cube can be mounted, as shown in figure 1 (a) and (b), which needs to be removed to allow transmitted light to pass through for bright field imaging. The filter cube can holder accommodates a 25.5×36 mm dichroic mirror and 25 mm diameter excitation and emission filters. These commonly used sizes allow convenient changing of the

optical filters with other microscopes according to experimental requirements.

The filter cube used here in layer 3 contains a bespoke multi-line dichroic beam splitter (ZT405/462/635/830rpc-UF2, [339819]) with matching emission filter (ZET405/462/635/830m, [339636]) and can be used with excitation filter (ZET405/465/625/825x) from Chroma technology. Alternatively, individual band pass excitation filters can be used. This specific dichroic beam splitter and emission filter combination are designed to work with single or multiwavelength excitation at 405 nm, 462 nm, 635 nm and transmit emission within bands at 408-457 nm, 472-627 nm, and 645-820 nm. The dichroic beam splitter also reflects radiation above 820 nm, which can be used for an optical autofocus system[13].

To provide excitation radiation for fluorescence microscopy, we assembled a computer-controlled laser bank of multimode diode lasers to provide switchable excitation at multiple wavelengths, as indicated in figure 2. The laser bank includes 4 multi-mode diode laser modules (LDM-638-700-C, LDM-520-1000-C, LDM-462-1400-C, LDM-405-350-C, Lasertack GmbH), labeled DL 1 – DL 4, providing multimode continuous wave laser radiation centered on wavelengths of 638 nm, 520 nm, 462 nm and 405 nm with maximum powers of ~700 mW, ~1000 mW, ~1400 mW and ~350 mW, respectively. To block amplified spontaneous emission and ensure narrowband excitation, e.g., for use with our multiline dichroic beam splitter and emission filter, we use four band pass filters (#65106, #65093, #39308, #65072, Edmund Optics), labeled as BP 1 – BP 4, each of 10 nm FWHM (full width at half maximum) and place them in front of the respective diode laser module outputs. A suitable combination of 3 dichroic beam combiners labeled as DBC1, DBC2 and DBC3, (#86394, #86324, #86389, Edmund Optics), and 9 broadband dielectric mirrors (M 1 – M9, BB05-E02, Thorlabs) mounted in kinematic mounts steer the laser beams from the 4 diode lasers to be collinear at the lens L4, which focusses the laser radiation into a multimode optical fibre. The diode laser drivers, LD1 – LD4, (2.5 Ampere iLD Driver, Lasertrack GmBH), provide linear control of the laser powers via a steady control current that is regulated by modulating the driver voltages using four programmable Arduino microcontrollers [21,22], AD1 – AD4, each with an associated Analogue to Digital Converter (ADC), TLV5618AI, Texas Instruments. Each driver also provides temperature control via an integral thermoelectric cooler (TEC) driver, as well as an interlock mechanism. The µManager programme controlling the microscope can address these Arduino microcontrollers to control the fluorescence excitation. The components for this laser bank cost approximately 500,000 INR.

(E) **Tube lens**: Layer 2 in the *openFrame* stack houses a tube lens of 200 mm focal length **(**#58-520**,** Nikon), which relays the fluorescence or transmitted light from the objective lens to the camera.

(F) **Detection**: Layer 1 generally incorporates a silver-coated right-angled mirror (#89-632, Edmund Optics) mounted on the optical axis of the openFrame that reflects the incident light to a camera mounted on the side port of the layer. This unit houses two such mirrors on a mechanical slider that can be switched to direct the incident light to cameras mounted on ports on opposite sides of the layer. In the present configuration, we use only one such port that detects the light from the sample after being reflected from the right-angled mirror.

We use two newly available low-cost fan–cooled CMOS cameras: a monochrome camera (CellCam Centro 200MR, Cairn Research Ltd) primarily used for fluorescence imaging and a color CMOS camera (CellCam Rana 200CR, Cairn Research Ltd) primarily used for brightfield imaging with white light transillumination. Both cameras use the Sony IMX 183 CMOS sensor, which has a 5440×3648 array of 2.4 µm pixels, although the color filter mask on the color CMOS camera effectively reduces the number of pixels by 4.

Software: To control all the components of this brightfield cum fluorescence microscope via a personal computer interface we use *µManager* [21–24], a java-based open source software tool written for light microscopy that has a comprehensive list of device adapter software for various instrument/hardware components. Many commercial hardware components are supplied with a DLL (dynamic library link). Once the respective DLL file is installed, µManager provides the option to configure and control the hardware through its software control panel via the relevant device adapter software. For our system the *µManager* is configured to control the X-Y stage and the Z drive, image acquisition by the two cameras and modulation of the output power of the 4 excitation lasers. µManager has also options to configure and control the LED sources [25–27]. For image analysis, µManager can be used with the open source software, ImageJ [28], for which further functionality is available, as demonstrated by the open source software called FIJI [29].

3. Implementation of the *openFrame*-based Microscope

The complete *openFrame*-based optical microscope configuration used here is depicted in figure 3. This schematic indicates how the light from the diode lasers inside the laser bank is delivered to the excitation unit mounted on *openFrame* layer 3 via a multi-mode optical fibre (MMF) cable. The excitation unit comprises a fibre connector (SM1-FC/PC, Thorlabs) attached to a lens tube (SM105, Thorlabs) that contains lens L2, which collimates the excitation radiation emerging from the MMF and directs it to lens L1, which focusses it to the back focal plane of the microscope objective lens. The MMF is vibrated to mix the spatial modes of the radiation and causes any speckles formed in the illuminated area of the sample plane to be time-averaged to provide spatially uniform illumination. This uniform illumination is provided over ~125 µm, 315 µm and 630 µm diameter circular fields of view (FOV), using the 100X,

40X and 20X microscope objective lenses respectively. The illuminated area of the sample plane depends on the NA of the MMF. In our case, the NA of the MMF with a 50 µm core (FG050UGA-CUSTOM, Thorlabs) is 0.22. This arrangement is able to deliver up to 90% of the laser power to the objective back aperture.

4. Results and discussion

4.1. Brightfield imaging using transmitted light

To demonstrate the *openFrame*-based microscope in the trans-illumination mode, we imaged a positive 1951 USAF test target (R3L3S1P, Thorlabs). The image acquisition was controlled using the *µManager* program and the captured images were analyzed in *FIJI*. Figure 4 (a) shows the image of the test target using the 20X objective lens while figures 4 (b) and (c) show the images of the same target using the 100X objective lens with immersion oil. The target comprises a number of patterns of opaque strips including the patterns for Group 7, Element 1 (G7E1), and G7E6, indicated as regions of interest (ROI) by yellow rectangles. We plotted the gray scale intensity profiles against the pixel number along a line normal to the strips and from each line profile we calculated the FWHM of the opaque and transparent strips inside the particular ROI.

We then take the estimated values and compare them with the corresponding width as specified by the manufacturer. Table 1 shows that the measured mean FWHM of the strips are in reasonable agreement with the values in the supplied specification – confirming that the microscope and the camera are reasonably well configured.

4.2. Imaging using the epi-fluorescence mode (multiwavelength excitation)

To demonstrate the epi–fluorescence mode of this *openFrame*-based microscope with multiwavelength excitation, we image a mixture of crimson red (F8806 FluoSpheres® carboxylate, Invitrogen™) fluorescence beads of particle size 220 nm and orange–green (F8809 FluoSpheres® carboxylate, Invitrogen™) fluorescence beads of particle size 200 nm, diluted in deionized water and kept in between a cover glass and a microscope glass slide. The crimson red beads can be predominantly excited using the 638 nm laser while the orange–green beads can be predominantly excited using the 462 nm laser. We first use the 100X objective lens and the fluorescence filter cube in layer 3 to image the specimen slide excited with the 638 nm and 462 nm diode lasers when switched on simultaneously and record the image using the color (CellCam Rana 200CR colour CMOS) camera shown in figure 5 (a). The multiline dichroic beam splitter and filter set allows fluorescence light from the beads excited by both the 638 nm and 462 nm radiation to be imaged simultaneously. We then excite the same region on the slide using the 462 nm diode laser and the image of the respective

beads is shown in figure 5 (b). We then switch on the 638 nm diode laser and the image of the respective beads is shown in figure 5 (c). Figure 5 illustrates this multispectral epi-fluorescence modality of the *openFrame*-based microscope using dual excitation wavelengths, showing both the crimson red beads with orange color and orange-green beads with light green color.

4.3. Comparison with a standard commercial microscope for the bright-field and epi-fluorescence modes

We compared the performance of the *openFrame*-based microscope with a standard commercial fluorescence microscope (IX51, Olympus) in the epi-fluorescence mode by imaging carboxyl quantum dots (QDs), (Q21361MP, Invitrogen™) that were diluted in deionized water and mounted between a microscope glass slide and a cover glass. In both the microscopes we excited the QDs with the 462 nm wavelength laser and use the same monochrome CMOS camera and filter set to record fluorescence images detected in the wavelength range 650-850 nm. These QDs have diameters ranging between 15 – 20 nm, i.e., much smaller than the excitation or the emission wavelengths and hence their image can directly provide the lateral PSF of the respective microscope [30]. For each fluorescence microscope, we imaged the QD using a research grade 100X oil immersion objective lens (UPlanSApo, 1.40 N.A., Olympus, with a cost of ~400,000 INR) and a cheaper (with a cost of ~60,000 INR) 100X Plan Fluor oil immersion lens (PF100X-INF, 1.3 NA, AmScope).

We first imaged the QD with the Olympus IX51 microscope using the Olympus 1.4 NA objective lens and then imaged another area of the QD slide with the AmScope 1.3 NA objective lens, for which Figures 6 (i) (a) and (b) show the respective images. We then imaged different areas of the QD slides using same two objective lenses in the *openFrame*-based microscope, for which Figures 6 (i) (c) and (d) show the respective images.

From each image in figure 6 we select a random set of isolated QDs and plot intensity vs position through the centre of images of isolated QD. Figures (ii) (a-d) show the raw and the Gaussian fitted line plot for a particular isolated QD taken from figures (ii) (a-d), respectively. The mean FWHM of the line plot for each image provides a measure of the experimental lateral PSF. The lateral FWHM of the theoretical diffraction-limited PSF is 0.51 λ/NA [31]. Table 2 presents the comparison of the mean lateral FWHMs of the experimental PSFs of 8 QDs in each case, and theoretical prediction for the two objective lenses.

Table 2 shows that the experimentally obtained lateral PSF is not significantly different when measured on either microscope using the same excitation wavelength, camera, filter set and objective lens, and that using the low-cost 1.3 NA AmScope objective lens provides a resolution only ~5% worse than that obtained using the more expensive 1.4 NA Olympus objective lens. Note that, in general, the lateral FWHM of a lens with 1.3 NA should theoretically be ~7.7% wider than that of a lens with 1.4 NA. Table 2 shows that the *openFrame*-based microscope with a low-cost objective lens provides comparable image quality with a commercial microscope using the same objective lens and that the openFrame-based and commercial (Olympus) microscopes also provide similar lateral FWHM when using the same (Olympus) objective lens of the same numerical aperture. We then imaged a specimen slide of unstained human glioblastoma cells (U87MG) using both the bright-field and epi-fluorescence modes to compare images acquired using the *openFrame*–based microscope and the commercial optical microscope (IX51, Olympus). Here we used a PlanF 40X 0.75 N.A., (PF40X-INF, AmScope) lens in the *openFrame*-based microscope and 40X, 0.60 N.A. (LUCPlanFLN, Olympus Optical) in the Olympus IX51 microscope, while using the same color CMOS camera and filter cube in both systems. Figures 7(i)(a) and (c) show the bright-field images of two different areas from the specimen, obtained using the Olympus microscope in the trans-illumination mode and figures 7(ii)(a) and (c) show the respective bright-field images of the same area when imaged with our *openFrame*-based microscope without any filter cube. We further investigate the autofluorescence by exciting the same area on the specimen slide with 462 nm diode laser and imaging in the epi-fluorescence mode using both the Olympus IX51 microscope and the *openFrame*-based microscope. The recorded autofluorescence images using the Olympus IX51 microscope are seen in figures 7(i)(b) and (d) while those acquired using the *openFrame*-based microscope are seen in figures 7(ii)(b) and (d). We see that the cells auto fluoresce in the light yellowish range with 462 nm laser excitation in the epi-fluorescence mode. Figure 7 demonstrates that performance of the *openFrame*-based microscope is similar to that of the Olympus IX51 fluorescence microscope. The fluorescence images acquired on the *openFrame*-based microscope are expected to be dimmer because the fluorophores in the field of view would already have undergone photobleaching during the fluorescence image acquisition on the Olympus microscope..

4.4. Clinical application (histopathological analysis)

We explored the use of the *openFrame*-based microscope in the trans-illumination and epi-fluorescence modes for clinical application by imaging specimen slides of human breast tissue sections stained with hematoxylin and eosin (H&E) [32,33] to detect normal and cancerous regions. Figure 8 (i) (a) shows the trans-illumination image of normal ducts

while figure 8 (i) (b) shows cancerous ducts from human breast tissue sections imaged using a standard optical microscope in the Pathology Department at Dr. B. Borooah Cancer Institute, Guwahati 781016 (based on an Eclipse 50i, NIKON) with a 40X objective lens (Nikon Plan, 40X/0.65 NA). In figure 8 (i) (a) the normal ducts present elliptical rings of epithelial cells inside them, while the image of cancerous duct in figure 8 (i) (b) shows infiltration into nearby ducts and into the cytoplasmic regions. Further, the regular rings of the epithelial cells are distorted, and many tumor cells appear inside the duct. The same H&E stained normal and cancerous human breast tissue sections are then imaged using the *openFrame*-based microscope, first using the trans-illumination mode with the 20X objective lens (Olympus PLN 20X/0.40 NA) and the color CMOS camera (without the filter cube).

Figure 8(ii)(a) shows the trans-illumination H&E image of a normal duct (inside the dashed circle), while figure 8(ii)(b) shows the trans-illumination H&E image of a cancerous duct (indicated by the dashed circle). As seen in figure 8(i)(a), the image of the normal duct in figure 8(ii)(a) shows an elliptical ring of epithelial cells. On the other hand, the duct seen in figure 8(ii)(b) is full of tumor cells and no regular rings of epithelial cells are seen.

The epi-fluorescence images in figures 8 (iii) (a) and (b) correspond to the same fields of view as figures 8 (ii) (a) and (b) and are excited using the 462 nm laser (with the customized multi-line beam splitter and the matching emission filter inside the filter cube in layer 3). Comparing the epi-fluorescence images with their respective trans-illumination images, it is clear that the stained cells in the cytoplasmic region as well as inside the duct fluoresce in green, while there is no fluorescence from the lumen region. This provides a sharp contrast to the boundary of the normal duct against the surrounding regions. As reported previously [34,35], we note that the green emission is a characteristic of the eosin dye, while the hematoxylin shows significant absorbance in the UV-VIS region with negligible emission in this range. The epi-fluorescence image in figure 8(iii)(b) shows that in the case of a cancerous duct, its boundary is indicated by a dark ring.

Another optical method which is considered useful for clinical diagnosis is optical coherence tomography (OCT) [36] which can provide three-dimensional volume information of tissue and is being explored for different applications, including generation of H&E-like images of fresh tissue [37]. Full-field OCT (i.e. FF-OCT) techniques can be implemented on any optical microscope including the openFrame-based instrument presented here if suitably adapted. Liu et al recently presented an implementation of FF-OCT on an openFrame-based microscope [38].

5. Component costs of the *openFrame*-based Microscope

In Table 3 we list the key components necessary to build the modular *openFrame*-based microscope in column 1 and an estimate of their total price in rupees in column 2. Note that these price estimates were made in 2020 before the pandemic. This list includes the motorized X-Y stage and the joystick which costs nearly 700,000 INR. In addition, we have included the price of 2 CMOS cameras (approx. 100,000 INR per item), the 100X oil immersion objective lens (approx. 60,000 INR) and the dichroic beam splitter and-emission filters (approx. 80,000 INR) for epi-fluorescence microscopy. However, instead of the motorized X-Y stage, one may also use a manual X-Y stage (e.g., manual Olympus XY Stage, CS S2001, Thorlabs). One could also image with a single camera.

6. Summary

We have presented the implementation of a cost-effective modular research-grade optical microscope implemented on an *openFrame*-based microscope stand. We have described the key components of the *openFrame*-based microscope: the main body of the microscope made of anodized aluminium, including the base, four modular layers accommodating the objective lens, scanning stage, fluorescence filter cube, tube lens and camera turning mirror, a trans-illumination pillar, and the excitation laser bank. The modular nature and low cost of components, combined with the use of open-source software, facilitate straightforward and affordable maintenance of the entire microscope.

We have shown the ability to operate this *openFrame*-based microscope in the trans-illumination mode using an LED trans-illumination source or in the epi-fluorescence mode using two different excitation lasers. We have demonstrated research-grade imaging performance of the *openFrame*-based microscope and have indicated its potential for clinical histopathological analysis through the application to human breast tissue sections. The modular form of *openFrame*-based microscopes makes them easily adaptable to other modalities. While here we have only implemented conventional brightfield and epifluorescence microscopy, the same microscope could be configured as a super-resolving microscope using *easy*STORM [13,17] or adapted to quantitative phase microscopy [16]. This open approach to microscope hardware and software enables systems to be assembled and maintained locally in a wide range of laboratory settings, which could widen access to optical microscopy. The *openFrame*-based microscope in the trans-illumination mode can be easily converted to a phase contrast microscope by incorporating an annular mask below the LED source and in the back focal plane of the condenser lens, and using a phase contrast objective lens in layer 4. Alternatively, we can insert a quadrant polariser mask in the back focal plane of the condenser lens and capture an image of the sample with a polarization-

resolving camera to reconstruct quantitative phase images of the sample after appropriate post processing of the four polarisation-resolved images extracted from the captured image as already demonstrated in an openFrame-based microscope[16]. The performance of any optical microscope can be limited by optical aberrations including openFrame-based microscopes. The modular flexibility of the openFrame enables an adaptive optics system to be implemented, e.g., compensate for specimen induced aberrations. For example, it would be possible to replace the right-angled mirror in layer 1, with a deformable mirror to implement a sensor less genetic algorithm based adaptive optics system [39].

Acknowledgements

The author A.B., would like to acknowledge the Department of Higher Education, Ministry of Education (MoE), GoI, for the financial support in the form of a monthly scholarship. A.K. would like to thank the Indian Institute of Technology Guwahati, for financial support in terms of an Institute Post-Doctoral Fellowship (IPDF).

Conflict of interest statement:

The *openFrame* concept originated at Imperial College London and has been co-developed with Cairn Research Ltd (and sister company, Cairn GmbH). An *openFrame*-based microscope similar to that reported in this paper can be constructed using components fabricated according to CAD files available at https://www.imperial.ac.uk/photonics/research/biophotonics/instruments--software/fluorescence-microscopy/openframe/, or these components can be purchased from Cairn Research Ltd. for users who wish to assemble their own instruments but not to fabricate the components themselves. Cairn also designs and sells bespoke application-orientated openFrame-based instruments combining open-source components with proprietary Cairn and third-party components.

References

1. Sampedro, A. and Howard, V., Cell Biological Applications of Confocal Microscopy. Edited by Brian Matsumoto. *J. Microsc.*, 1994, **175**, 91–92.
2. Jacquemet, G., Carisey, A. F., Hamidi, H., Henriques, R., and Leterrier, C., The cell biologist's guide to super-resolution microscopy. *J. Cell Sci.*, 2020, **133**.
3. Halbhuber, K.-J. and König, K., Modern laser scanning microscopy in biology, biotechnology and medicine. *Ann. Anat. - Anat. Anzeiger*, 2003, **185**, 1–20.
4. Wollman, A. J. M., Muchová, K., Chromiková, Z., Wilkinson, A. J., Barák, I., and Leake, M. C., Single-molecule optical microscopy of protein dynamics and computational analysis of images to determine cell structure development in differentiating Bacillus subtilis. *Comput. Struct. Biotechnol. J.*, 2020, **18**, 1474–1486.

5. König, K., Multiphoton microscopy in life sciences. *J. Microsc.*, 2000, **200**, 83–104.

6. Borst, J. W. and Visser, A. J. W. G., Fluorescence lifetime imaging microscopy in life sciences. *Meas. Sci. Technol.*, 2010, **21**, 102002.

7. Yao, N. and Wang, Z. L., Handbook of microscopy for nanotechnology. 2005.

8. Johnson, S. A., Nanoscopy for nanoscience: how super-resolution microscopy extends imaging for nanotechnology. *WIREs Nanomedicine and Nanobiotechnology*, 2015, **7**, 266–281.

9. Poola, P. K., Afzal, M. I., Yoo, Y., Kim, K. H., and Chung, E., Light sheet microscopy for histopathology applications. *Biomed. Eng. Lett.*, 2019, **9**, 279–291.

10. U, A. D. and Mazumder, N., Types of advanced optical microscopy techniques for breast cancer research: a review. *Lasers Med. Sci.*, 2018, **33**, 1849–1858.

11. Garcia, E., Lightley, J., Kumar, S., et al., Application of direct stochastic optical reconstruction microscopy (dSTORM) to the histological analysis of human glomerular disease. *J. Pathol. Clin. Res.*, 2021, **7**, 438–445.

12. https://www.imperial.ac.uk/photonics/research/biophotonics/instruments--software/fluorescence-microscopy/openframe/.

13. Lightley, J., Kumar, S., Lim, M. Q., et al., openFrame : A modular, sustainable, open microscopy platform with single-shot, dual-axis optical autofocus module providing high precision and long range of operation. *J. Microsc.*, 2023, https://doi.org/10.1111/jmi.13219.

14. https://github.com/ImperialCollegeLondon/openFrame.

15. *openFrame components can be purchased from Cairn Research Ltd, https://www.cairn-research.co.uk/product/openframe-microscope/.*

16. Kalita, R., Flanagan, W., Lightley, J., et al., Single-shot phase contrast microscopy using polarisation-resolved differential phase contrast. *J. Biophotonics*, 2021, **14**, e202100144.

17. Kwakwa, K., Savell, A., Davies, T., et al., easySTORM: a robust, lower-cost approach to localisation and TIRF microscopy. *J. Biophotonics*, 2016, **9**, 948–957.

18. Rust, M. J., Bates, M., and Zhuang, X., Sub-diffraction-limit imaging by stochastic optical reconstruction microscopy (STORM). *Nat. Methods*, 2006, **3**, 793–796.

19. Heilemann, M., van de Linde, S., Schüttpelz, M., et al., Subdiffraction-Resolution Fluorescence Imaging with Conventional Fluorescent Probes. *Angew. Chemie Int. Ed.*, 2008, **47**, 6172–6176.

20. Lightley, J., Görlitz, F., Kumar, S., et al., Robust deep learning optical autofocus system applied to automated multiwell plate single molecule localization microscopy. *J. Microsc.*, 2022, **288**, 130–141.

21. Edelstein, A. D., Amodaj, N., Hoover, K., Vale, R. D., and Stuurman, N., Computer Control of Microscopes Using μManager. *Curr. Protoc. Mol. Biol.*, 2010, **92**.

22. Arduino, https://www.arduino.cc/.

23. Stuurman, N., Adapter for the Arduino electronics prototyping platform.

24. Edelstein, A. D., Tsuchida, M. A., Amodaj, N., Pinkard, H., Vale, R. D., and Stuurman, N., Advanced methods of microscope control using $μ$Manager software. *J. Biol. methods*, 2014, **1 2**.

25. https://www.cairn-research.co.uk/product/89-north-ldi-support-in-micromanager-test/.

26. https://www.coolled.com/wp-content/uploads/2014/04/MicroManager-Software-Summary-Sheet-R3.pdf.

27. https://www.thorlabs.com/newgrouppage9.cfm?objectgroup_id=3832.

28. Schneider, C. A., Rasband, W. S., and Eliceiri, K. W., NIH Image to ImageJ: 25 years of image analysis. *Nat. Methods*, 2012, **9**, 671–675.

29. Schindelin, J., Arganda-Carreras, I., Frise, E., et al., Fiji: an open-source platform for biological-image analysis. *Nat. Methods*, 2012, **9**, 676–682.

30. YOO, H., SONG, I., and GWEON, D.-G., Measurement and restoration of the point spread function of fluorescence confocal microscopy. *J. Microsc.*, 2006, **221**, 172–176.

31. WILSON, T., Resolution and optical sectioning in the confocal microscope. *J. Microsc.*, 2011, **244**, 113–121.

32. Alturkistani, H. A., Tashkandi, F. M., and Mohammedsaleh, Z. M., Histological Stains: A Literature Review and Case Study. *Glob. J. Health Sci.*, 2015, **8**, 72.

33. Fischer, A. H., Jacobson, K. A., Rose, J., and Zeller, R., Hematoxylin and Eosin Staining of Tissue and Cell Sections. *Cold Spring Harb. Protoc.*, 2008, **2008**, pdb.prot4986.

34. Gibbs, Summer L; Genega, Elizabeth; Salemi, Jeffery; Kianzad, Vida; Goodwill, Haley L.; Xie, Yang; Oketokoun, Rafiou; Khurd, Parmeshwar; Kamen, Ali; Frangioni, J. V., Multiphoton microscopic imaging of histological sections without hematoxylin and eosin staining differentiates carcinoma in situ lesion from normal oesophagus. *Mol. Imaging*, 2015, **15**.

35. Gibbs, S. L., Genega, E., Salemi, J., et al., Near-Infrared Fluorescent Digital Pathology for the Automation of Disease Diagnosis and Biomarker Assessment. *Mol. Imaging*, 2015, **14**, 7290.2015.00005.

36. Bouma, B. (ed.), *Handbook of Optical Coherence Tomography* CRC Press, 2001.

37. Lin, S.-E., Jheng, D.-Y., Hsu, K.-Y., et al., Rapid pseudo-H&E imaging using a fluorescence-inbuilt optical coherence microscopic imaging system. *Biomed. Opt. Express*, 2021, **12**, 5139.

38. Liu, H., Valand, K., Kumar, S., et al., Single-Shot Semi-Quantitative Phase Contrast Microscopy. In *Focus on Microscopy conference Oporto, Portugal* 2023.

39. Tehrani, K. F., Xu, J., Zhang, Y., Shen, P., and Kner, P., Adaptive optics stochastic optical reconstruction microscopy (AO-STORM) using a genetic algorithm. *Opt. Express*, 2015, **23**, 13677.

Table 1. Measured width of a strip in the G7E1 and G7E6 patterns of the 1951 USAF resolution test chart using different objective lenses in the trans-illumination mode.

Pattern name	Specified width of a black strip (µm)	Measured width of a black strip with different objective lenses (µm)	
		20 X 0.4 N.A.	100 X oil immersion 1.3 N.A.
G7E1	3.91	3.99	3.92
G7E6	2.19	2.31	2.2

Table 2. Theoretically and experimentally obtained FWHM of the lateral PSF for the standard optical microscope and the openFrame-based microscope using the same two objective lenses.

QD type	QD size	FWHM of lateral PSF (theory) using λ=705 nm		Mean FWHM of lateral PSF measured using CMOS camera (with 2.4μm pixel size corresponding to 24 n in sample plane)			
		1.4 N.A. 100x objective lens	1.3 N.A. 100x objective lens	Standard Commercial Microscope		*openFrame*-based Microscope	
				1.4 N.A. 100x Olympus lens	1.3 N.A. 100x AmScope lens	1.4 N.A. 100x Olympus lens	1.3 N.A. 100x AmScope lens
Carboxyl Quantum Dots Peak emission at 705 nm	15 - 20 nm	256 nm	276 nm	310 ± 3 nm	328 ± 2 nm	311 ± 4 nm	324 ± 3 nm

Table 3. A rough estimate of the price of the components that goes into building the *openFrame*-based microscope.

	Components name	Approx. price (in Indian rupees)
1	Excitation and camera ports components 1.3 N.A. oil immersion 100X objective	200,000
2	Despeckler and power supply Transillumination pillar & LED source PI piezo stage with controller CellCam 200MR CellCam 200CR Zaber motorized X-Y stage with controller	1,250,000
3	openFrame modular stand	300,000
4	405 nm diode laser (with laser driver) 462 nm diode laser (with laser driver) 520 nm diode laser (with laser driver) 638 nm diode laser (with laser driver)	134,000
5	Electronics and metal boxes for diode laser control Mirrors, DBC and Optical filters Mounts, posts, screw and other components inside laser bank	280,000
	Total (gross) price:	2,164,000

Figure 1: (a) Schematic of the openFrame-based microscope showing the four layers, base plate, X-Y sample stage, trans-illumination pillar and other hardware components and (b) CAD representation of the openFrame modular microscope stand and a single layer with the cube insert.

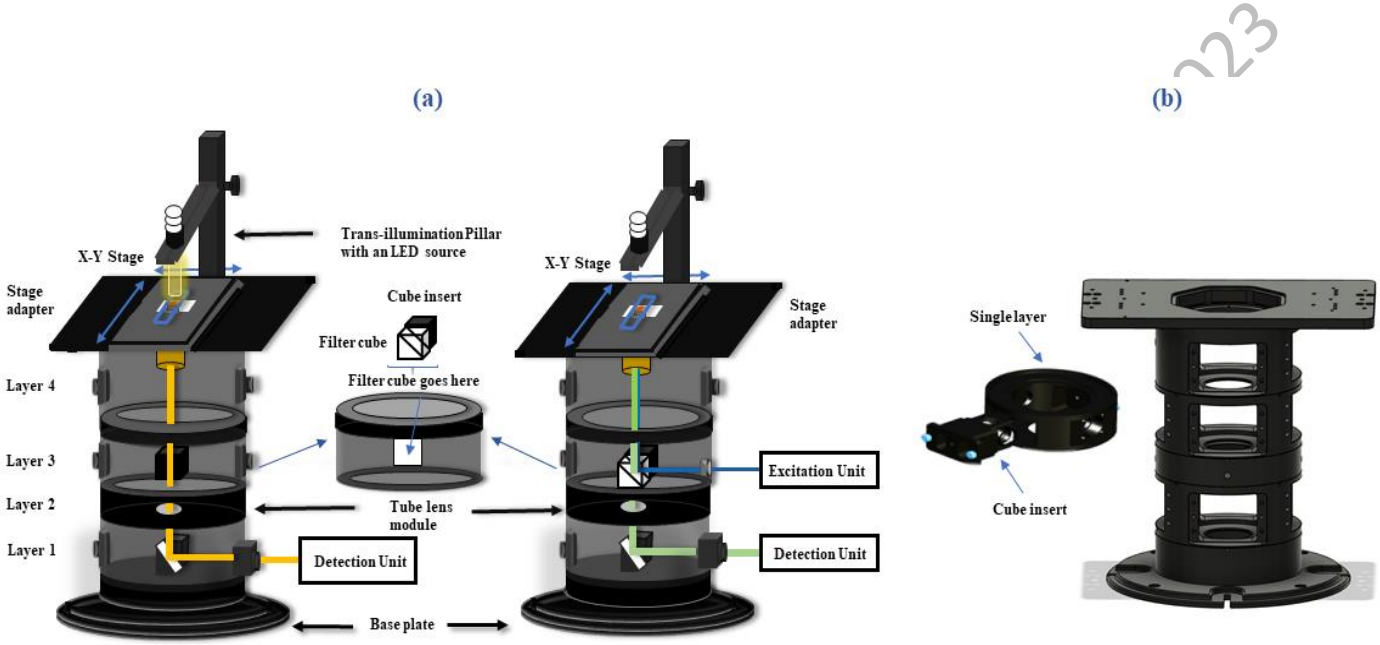

Figure 2: A schematic of the PC controlled LASER BANK equipped with the lasers, optics and electrical components which is a part of the excitation unit.

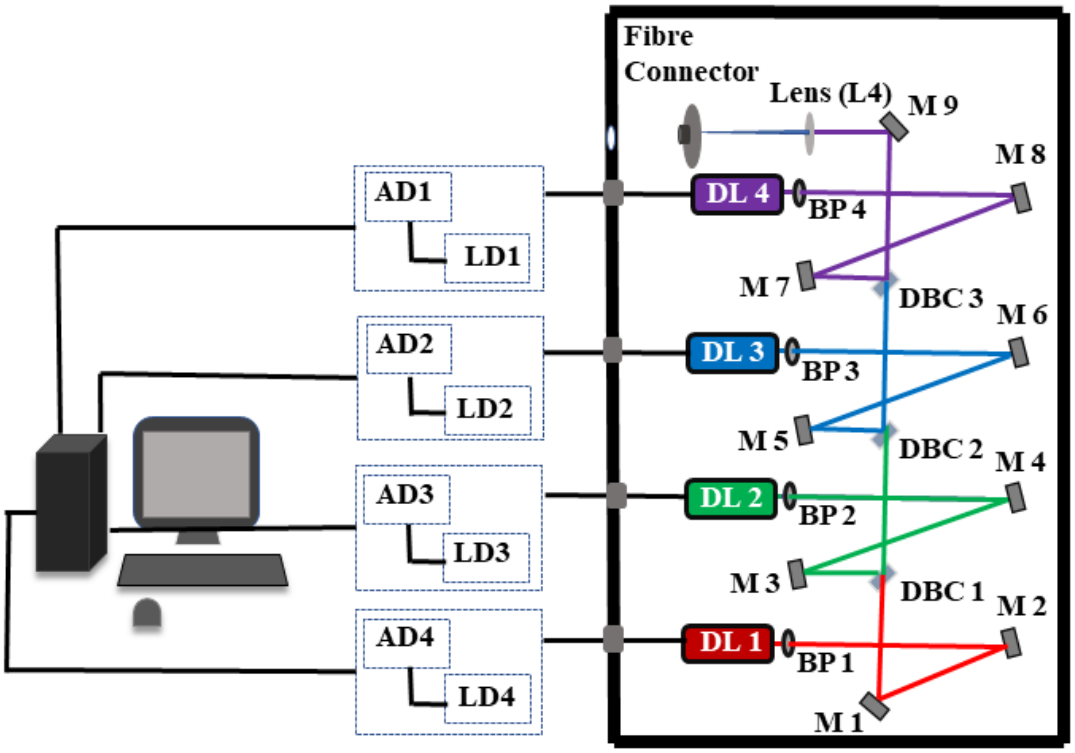

AD1 – AD4 : Arduino Boards
BP 1 – BP 4 : Band Pass Filters
DBC 1- DBC 3 : Dichroic Beam Combiners
DL 1- DL 4 : Diode Lasers
LD1 – LD4 : Laser Drivers
M 1-M 9 : Mirrors

Figure 3: A schematic of the complete openFrame-based microscope implemented by assembling the necessary hardware, optical, opto-electronic and electronic components.

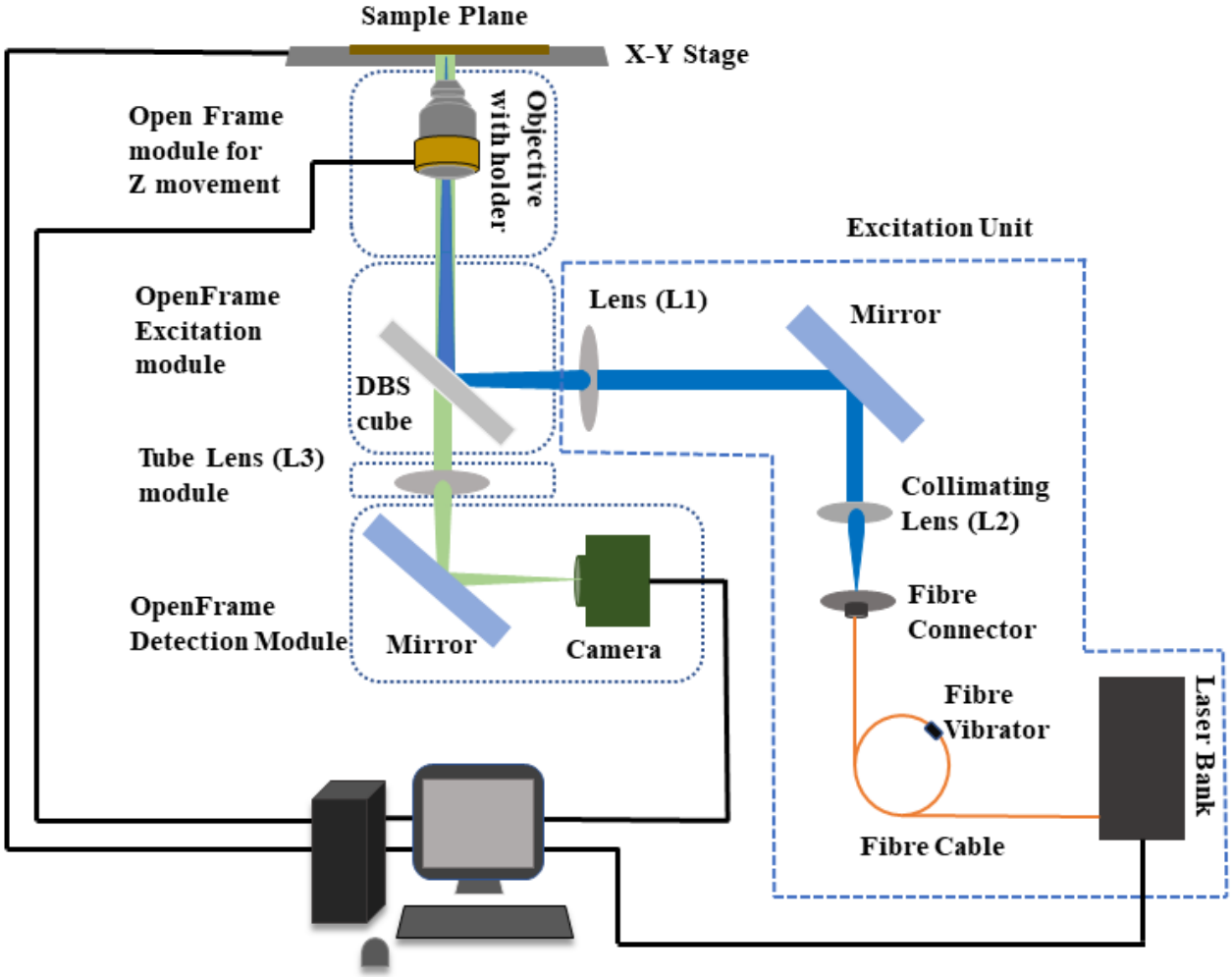

Figure 4: Trans-illumination images of a 1951 USAF test target (a) with the 20X objective lens, (b) with the 100X objective lens showing the G7E1 pattern, and (c) with the 100X objective lens showing the G7E6 pattern, captured by the monochrome camera. The yellow rectangles on the two groups indicate the directions in which line profiles are drawn for estimating the width of the respective strips.

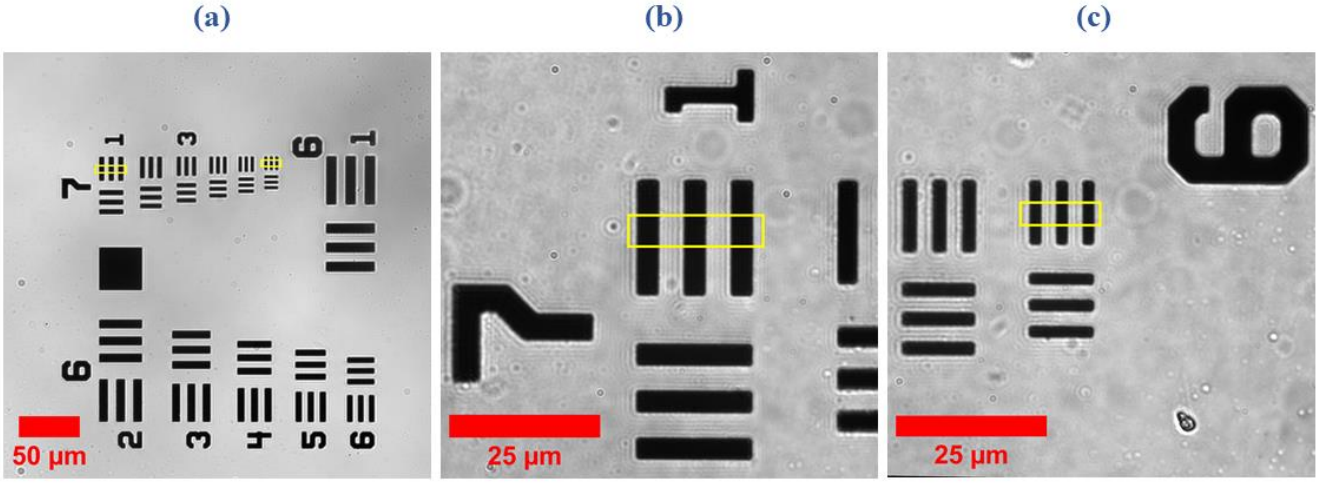

Figure 5: Epi–fluorescence images of the specimen slide containing a mixture of crimson red and orange-green fluorescent beads, (a) excited with both 462 nm and 638 nm lasers, using the 100X objective lens on the colour CMOS camera, (b) excited with 462 nm laser, and (c) excited with 638 nm laser.

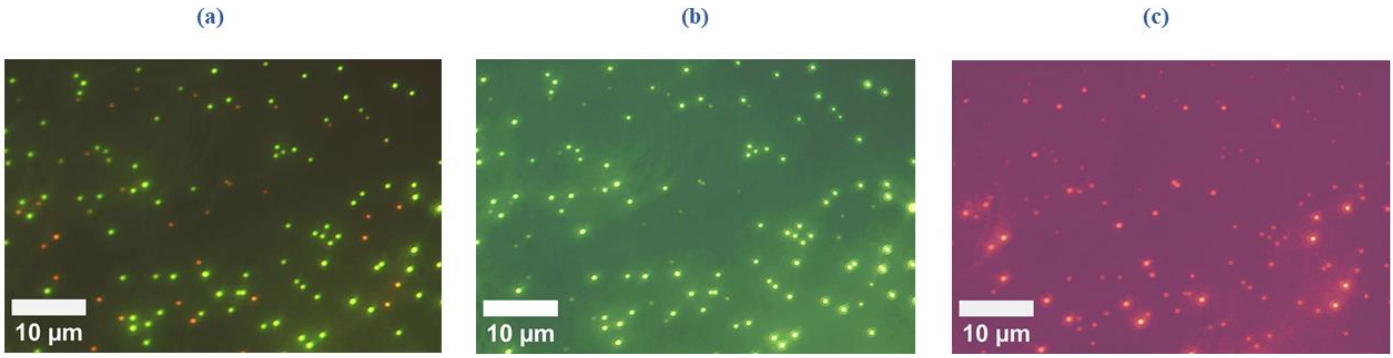

Figure 6: (i)(a) and (i)(b) show epi-fluorescence images of QDs on the monochrome CMOS camera obtained using the commercial (Olympus IX51) fluorescence microscope with 1.4 N.A. Olympus and 1.3 N.A. AmScope objective lenses, respectively. (i)(c) and (i)(d) show images of QDs acquired using the same monochrome CMOS camera obtained in the epi-fluorescence mode using the openFrame-based microscope with the same 1.4 N.A. Olympus and 1.3 N.A. AmScope objective lenses, respectively. (ii)(a), (b) and (ii)(c), (d) represent the plots of raw intensity data and the respective fitted line plots for an isolated QD chosen randomly from (i)(a), (b) and (i)(c), (d) respectively.

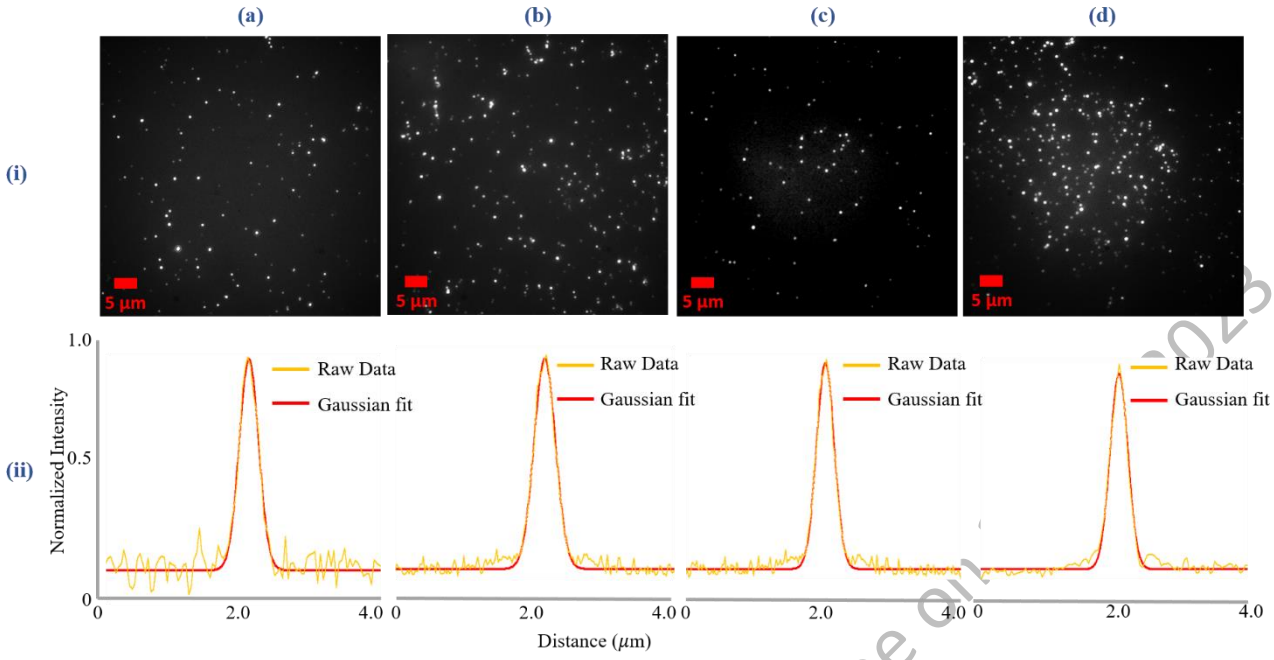

Figure 7: Top row shows brightfield (i)(a,c) and fluorescence (i)(b,d) images of two areas on the specimen slide of unstained human glioblastoma cells (U87MG) acquired on Olympus IX51 microscope with 40X, 0.60 N.A (LUCPlanFLN, Olympus) objective lens and bottom row shows brightfield (ii)(a,c) and fluorescence (ii)(b,d) images of the same fields of view acquired subsequently on the openFrame-based microscope with a low-cost 40X 0.75 N.A. (PF40X-INF, AmScope) objective lens. The brightfield images were acquired using the colour CMOS (CellCam Rana 200CR) camera and the fluorescence was excited at 462 nm and acquired using the same colour CMOS camera.

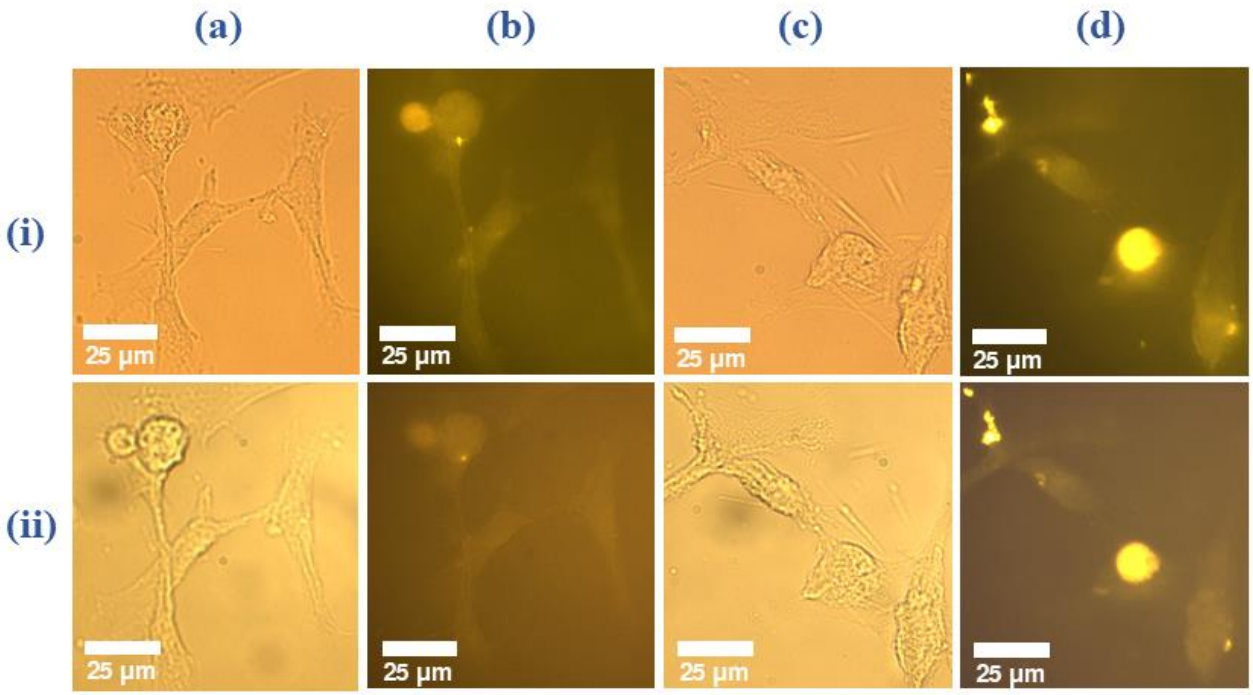

Figure 8: Trans-illumination brightfield images of H&E stained (i)(a) normal, (i)(b) cancerous human breast tissue sections under a commercial (Eclipse 50i, NIKON) microscope with a 40X objective lens acquired with colour CMOS (CellCam Rana 200CR) camera. Trans-illumination brightfield images of H&E stained (ii)(a) normal, (ii)(b) cancerous human breast tissue sections under openFrame-based microscope with 20X objective lens acquired with the same colour CMOS camera. The epi-fluorescence images, corresponding to (ii)(a) and (b), using 462 nm excitation laser, are seen in (iii)(a) and (b), respectively.